Slide-hold-slide experiments and frictional healing in a simulated granular fault gouge

Behrooz Ferdowsi[1], **Allan M. Rubin**[1]

[1]Department of Geosciences, Princeton University, Princeton, NJ 08544, USA

Key Points:

- We examined the behavior of a sheared granular layer with time-independent contact-scale properties in slide-hold-slide protocols.
- The slide-hold simulations with different model stiffnesses mimic the stress decay response of laboratory friction data.
- The long-time slope of the log-time healing (the peak stress upon resliding) is nearly equal to the rate-state friction "b" value.

Corresponding author: Behrooz Ferdowsi, `behrooz@princeton.edu`

Abstract

The empirical constitutive modeling framework of Rate- and State-dependent Friction (RSF) is commonly used to describe the time-dependent frictional response of fault gouge to perturbations from steady sliding. In a previous study (Ferdowsi and Rubin, 2020), we found that a granular-physics-based model of a fault shear zone, with time-independent properties at the contact scale, reproduces the phenomenology of laboratory rock and gouge friction experiments in velocity-step and slide-hold protocols. A few slide-hold-slide simulations further suggested that the granular model might outperform current empirical RSF laws in describing laboratory data. Here, we explore the behavior of the same model in slide-hold and slide-hold-slide protocols over a wide range of sliding velocities, hold durations, and system stiffnesses, and provide additional support for this view. We find that, as is the case for laboratory data, the rate of stress decay during slide-hold simulations is in general agreement with the "Slip law" version of the RSF equations, using parameter values determined independently from velocity step tests. During reslides, the model, similar to lab data, produces a nearly constant rate of frictional healing with log hold time, at long hold times, with that rate being close to the RSF "state evolution" parameter b, consistent with the "Aging law" version of the RSF equations. We also find that, as in laboratory experiments, the granular layer undergoes log-time compaction during holds. This is consistent with the traditional understanding of the Aging law, even though the associated stress decay is similar to that predicted by the Slip and not the Aging law.

1 Introduction

The constitutive framework of Rate- and State-dependent Friction is often used for modeling transient frictional behavior of rocks and other Earth materials (e.g., sediment, glacial till), and for simulating frictional instabilities relevant to earthquakes, landslides and earthflows (J. H. Dieterich, 1992, 1978, 1979; J. H. Dieterich et al., 1981; Ruina, 1983; J. Dieterich, 1994; Marone, 1998; J. H. Dieterich & Kilgore, 1996; Viesca, 2016; Handwerger et al., 2016; McCarthy et al., 2017). A complete prescription of RSF requires an equation for the evolution of the "state variable" defining the state of the sliding interface. Existing versions of this equation are largely empirical, differ fundamentally in the extent to which slip or elapsed time is responsible for state evolution, and fail to satisfactorily match the suite of laboratory experiments they were designed to describe.

A popular concept has been that in the absence of sliding, state evolution (frictional strengthening, in such cases) is fundamentally a time-dependent process (J. H. Dieterich, 1972). This hypothesis has received support first from the observed logarithmic-with-time growth of contact area between transparent samples of PMMA (Polymethyl methacrylate), due to plastic deformation of contacting asperities (J. H. Dieterich & Kilgore, 1994), and more recently from the logarithmic-with-time increase in acoustic transmissivity across frictional interfaces in rock (Nagata et al., 2012). Log-time frictional strengthening of stationary surfaces has been shown to also result from increased chemical bonding (Li et al., 2011). The log-time increase in both contact area and chemical bonding have been shown to have a sound theoretical basis (Berthoud et al., 1999; Baumberger & Caroli, 2006; Liu & Szlufarska, 2012). Such behavior is embodied in the "Aging" (or "Dieterich") equation for state evolution (Ruina, 1983). Despite its theoretical basis, however, the Aging law accurately describes almost no rock or gouge friction data other than the observed increase in "static" friction with the logarithm of hold time in laboratory slide-hold-slide experiments (as measured by the friction peak upon resliding).

In contrast, a second popular equation for state evolution (the "Slip" or "Ruina" law) has no well-established theoretical justification, but does a remarkably good job describing the results of laboratory velocity-step experiments, as well as the stress decay during the hold portion of slide-hold-slide experiments (Ruina, 1983; Nakatani, 2001; Bhattacharya et al., 2015, 2017). The Aging and Slip laws are asymptotically identical for small perturbations from steady-state sliding, but diverge as the sliding deviates further from steady state. Notably, unlike the Aging law, the Slip law predicts no state evolution in the absence of slip (it can still generate an increase in frictional strength

approximately as log "hold" time during slide-hold-slide experiments, due to the small amount of slip accompanying the stress decay during holds applied by an elastic testing machine).

The lack of a physics-based theory for transient friction of rock has motivated exploring the physical and chemical origins of rate-state friction in a variety of scientific communities, and has also brought significant attention to the contributions of the quantity (contact area) versus the quality (shear strength) of contact asperities to the state of a frictional interface (Li et al., 2011; Chen & Spiers, 2016; Tian et al., 2017, 2018; Thom et al., 2018). However, future investigations are needed to address the implications of asperity-scale (and often single-asperity-scale) observations for the transient frictional behavior at macroscopic and multi-asperity scales. In addition, more work is necessary to determine if any of the single-asperity-scale observations may reproduce or explain the transient frictional behavior of rock and gouge materials in the lab.

In a previous study, we simulated the transient frictional behavior of a sheared granular gouge layer with constant Coulomb friction at grain-grain contacts, using the discrete element method (Ferdowsi & Rubin, 2020). We used the granular-physics-based model to study the fault gouge response to velocity-stepping and slide-hold-slide (SHS) numerical simulations, in a system where all the relevant time dependence resulted from momentum transfer between the gouge particles, rather than time-dependent plasticity or chemical reactions at the contact scale. We note that laboratory experiments on even initially bare rock surfaces develop a granular gouge layer through mechanical wear, and that laboratory experiments show that the phenomenology of RSF is common to both those experiments that start with bare rock and those where gouge is used as the starting material (Marone, 1998). By not considering time-dependent plasticity or chemical reactions at the contact scale, we are throwing out what is traditionally thought to be the source of the rate- and state-dependence of friction. Nonetheless, our previous results indicate that the sheared granular model successfully reproduces the rock and gouge friction behavior observed in laboratory velocity-step tests. In that work we also investigated a very limited number of SHS tests. We found that the stress decay during the hold portions of those simulations were consistent with the predictions of the Slip law, which itself is largely consistent with the stress decay in laboratory slide-hold experiments. During the reslides, on the other hand, the simulations deviated from the Slip law prediction, and it did so in a manner that plausibly was more consistent with laboratory experiments. However, a more extensive study of SHS behavior in the granular model compared to laboratory rock friction observations was deferred to this work.

Here, we examine the frictional behavior of the granular-physics-based model of fault gouge in SHS protocols for a range of sliding velocities and system stiffnesses. These stiffnesses include those close the stiffnesses used in published laboratory experiments. A primary objective of this study is to further explore the extent to which a sheared granular model of fault gouge with no time-dependent plasticity at the grain contacts can explain rock friction data as observed in the lab. We further compare the predictions of the model against the Slip- and Aging-law descriptions of state evolution, and study the energetics of the granular model in the SHS protocol. We believe the simulation results and analyses reported here could also be useful for researchers working in the fields of granular physics, constitutive modeling of granular materials and complex fluids. The observations reported here are important for accurately modeling frictional instabilities at the interface of Earth materials (rocks, sediments, ice-rock, many of which having microstructures that are reminiscent of granular materials and similar complex fluids) near the Earth's surface.

2 Rate- and State-Dependent Friction background

The empirical constitutive modeling framework of rate- and state-dependent friction attempts to describe friction as a function of the sliding rate, V, and the "state variable", θ. In its simplest form, RSF is described by two coupled, first order, ordinary differential equations. The first describes the relation between friction μ, defined as the ratio of shear stress to normal stress, and the RSF variables:

$$\mu = \mu_* + a\log\frac{V}{V_*} + b\log\frac{\theta}{\theta_*} \, , \tag{1}$$

where μ_* is the nominal steady-state coefficient of friction at the reference velocity V_* and state θ_*. The coefficients a and b control the magnitude of velocity- and state-dependence of the frictional strength, respectively. The second equation describes the evolution of the state variable θ, the two most widely used forms being

$$\text{Aging Law:} \quad \frac{d\theta}{dt} = 1 - \frac{V\theta}{D_c} \tag{2}$$

$$\text{Slip Law:} \quad \frac{d\theta}{dt} = -\frac{V\theta}{D_c} \ln \frac{V\theta}{D_c} \tag{3}$$

where D_c is a characteristic slip distance (J. H. Dieterich, 1979; Ruina, 1983). Eq. 2 is often referred to as the Aging law since state can evolve with time in the absence of slip; Eq. 3 is referred to as the Slip law since state evolves only with slip ($\dot{\theta} = 0$ when $V = 0$).

Previous studies have demonstrated that neither the Aging law nor the Slip law adequately describes the full range of laboratory velocity-stepping and slide-hold-slide loading protocols (Beeler et al., 1994; Kato & Tullis, 2001). Velocity-stepping experiments with a sufficiently stiff system show that following a change in velocity, friction approaches its new steady-state value quasi-exponentially over a characteristic slip distance that is independent of both the magnitude and the sign of the velocity step (Ruina, 1983; Marone, 1998; Blanpied et al., 1998; Bhattacharya et al., 2015). This observation holds for both bare rock and gouge samples, and (by design) it is consistent with the Slip law prediction for the evolution of state (Ruina, 1983; Nakatani, 2001). However, in the Aging law version of state evolution, the slip weakening distance increases as the logarithm of the velocity jump for step velocity increases, and for step decreases the frictional strength recovery occurs over exceedingly small slip distances as the magnitude of the velocity reduction increases (because state is increasing with time rather than slip) . Both of these Aging-law predictions are completely inconsistent with laboratory velocity-step data (Nakatani, 2001).

The Aging law was introduced primarily to account for the observation that in SHS experiments, beyond a "cut-off time" that is typically of order 1 s, the peak stress upon resliding increases approximately as the logarithm of the hold time (J. H. Dieterich, 1979; J. H. Dieterich & Kilgore, 1994; Ruina, 1983). However, Bhattacharya et al. (2017) reanalyzed the experimental SHS data of Beeler et al. (1994), conducted using two different machine stiffnesses (and hence two different amounts of interfacial slip during the load-point hold, as the loading machine and rock sample elastically unload), and found that the log-time increase in peak stress upon resliding could be fit about as well by the Slip law as by the Aging law. Bhattacharya et al. (2017) further found that the nearly logarithmic-with-time stress decay during the load-point holds could be well modeled by the Slip law, which predicts relatively little state evolution owing to the small amount of slip. In contrast, this log-time stress decay is completely inconsistent with the Aging law, which predicts too much strengthening (state evolution) during the holds, and a rate of stress decay that approaches zero as hold time increases (for $a/b < 1$, as was the case in these experiments). Despite the failure of the Aging law to fit both velocity-step tests and slide-hold tests, most theoretical justifications for the evolution of state presuppose mechanisms of time-dependent healing as embodied by the Aging law (e.g., Baumberger et al., 1999). But even the Slip law is unable to model data from both the hold and reslide portions of SHS tests (Bhattacharya et al., 2017).

2.1 Granular rate- and state-dependent friction

Both the failures of existing RSF equations and their empirical nature motivated our previous study, in which we modeled the behavior of a granular gouge layer with no time-dependent plasticity at the grain-grain contact scale, using the discrete element modeling method (Ferdowsi & Rubin, 2020). We explored the frictional behavior of the gouge layer in velocity-step numerical experiments over a range of driving velocities ($V = 1 \times 10^{-4}$ to 2 m/s) and normal stresses ($\sigma_n = 1$ to 25 MPa). We further performed a limited number of slide-hold-slide granular simulations. Consistent with RSF and several earlier numerical studies of sheared granular layers, we found that in response to imposed velocity steps, there is an immediate "direct velocity effect" (i.e., an increase in friction in

response to a step velocity increase), followed by a more gradual "state evolution effect" where the sign of the friction change is reversed (Morgan, 2004; Hatano, 2009; Abe et al., 2002). Furthermore, the magnitudes of these direct and evolution effects are proportional to the logarithm of the velocity jump, with implied values of the RSF parameters a and b ($\sim$0.02) that are not far from lab values. We further observed that overall the behavior of the granular model appears be very similar to lab data for velocity step and slide-hold tests. In this respect, the model agrees well also with the Slip law for state evolution. The results of our preliminary granular SHS simulations further indicated that the peak stress upon the reslide exceeds the prediction of the Slip law, using the same parameters that fit the hold well. This is similar to behavior observed in lab data (Bhattacharya et al., 2017); however, to highlight the role of state evolution, those earlier simulations employed a very large system stiffness so that the sliding velocity was very nearly equal to the load-point velocity. This stiffness greatly exceeds those that can be achieved in the laboratory. In the current study we also use stiffnesses more similar to laboratory tests.

3 The computational model

Our Discrete Element Method (DEM) simulations are performed using the *granular* module of LAMMPS (Large scale Atomic/Molecular Massively Parallel Simulator), a multi-scale computational platform developed and maintained by Sandia National Laboratories (http://lammps .sandia.gov) (Plimpton, 1995). Our model consists of a packing of 4815 grains: 4527 in the gouge layer, and 288 in the top and bottom rigid blocks. The grains in the gouge layer have a polydisperse normal-like size distribution, with a diameter range $d = [1 : 5]$ mm and average diameter $D_{mean} = 3$ mm (Figure 1A). The granular gouge is confined between two parallel and rigid plates that are constructed from grains with diameter $d = 5$ mm. Grain density and Young's modulus are chosen equal to properties of glass beads (Table S1). The model domain is rectangular with periodic boundary conditions applied in the x and y directions. The size of the system in each direction is $L_x = L_y = 1.5L_z = 20 \, D_{mean}$. The system is initially prepared by randomly inserting (under
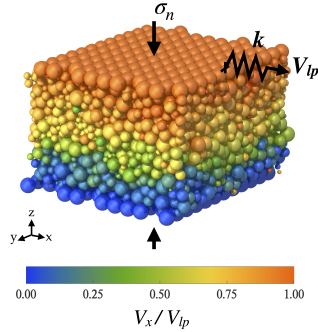

Figure 1. A visualization of the granular gouge simulation. Colors show the velocity of each grain in the x direction, averaged over an upper-plate sliding distance of D_{mean} during steady sliding at a driving velocity of $V_i = 2 \times 10^{-4}$ m/s.

gravity) grains in the simulation box with a desired initial packing fraction of $\sim$0.5. The system is then allowed to relax for about 10^6 time steps, after which it is subjected to confining pressures $\sigma_n = 5$ MPa. The confining pressure is applied for one minute, by which time the fast phase of compaction is completed. The confined gouge sample is then subjected to shearing at a desired driving velocity imposed by the top rigid plate, while the vertical position of the top wall is adjusted by a servo-control system to maintain the specified (constant) confining pressure. The driving velocity is applied to the system via a linear spring attached to the top plate with one of 3 stiffnesses: $k_{pull} = \{1 \times 10^{10}, 8 \times 10^5, 2.7 \times 10^4\}$ N/m. We will get back to the choices of the spring stiffness at the end of this section.

The grains are modeled as compressible elastic spheres of diameter d that interact when in contact via the Hertz-Mindlin model (Johnson, 1987; Landau & Lifshitz, 1959; Mindlin, 1949). Slip occurs at grain contacts when the local shear stress exceeds the specified (constant) local friction coefficient. Energy loss at contacts is characterized by the "restitution coefficient", which potentially varies from 0 (complete energy loss) to 1 (zero loss). At the low sliding speeds of interest the adopted value appears to have very little influence on the macroscopic behavior of the system (Ferdowsi & Rubin, 2020; MiDi, 2004). The full details of the granular module of LAMMPS are described in the LAMMPS manual and several references (Zhang & Makse, 2005; Silbert et al., 2001; Brilliantov et al., 1996). For the details of the implementation of the model in this manuscript, and a complete list of the governing dimensionless variables, we refer the reader to the "Computational Model" section and Appendix A of Ferdowsi and Rubin (2020). All details of the present model, except for the values of pulling spring stiffness or unless otherwise specified in the following, are identical to the "default" model of our previous paper.

The velocity V in the RSF equations (1)–(3) is interpreted in laboratory experiments as the inelastic component of the relative tangential displacement rate between two parallel planes. This displacement rate is typically treated conceptually as occurring across a plane of zero thickness, but in fact it occurs across a zone whose thickness is generally unknown. In lab experiments, the relative displacement is measured between two points outside the zone of inelastic deformation, and the inelastic component of that displacement δ is determined by subtracting the estimated elastic displacement δ_{el} from the measured (total) displacement, i.e.

$$
\begin{aligned}
\delta &= \delta_{lp} - \delta_{el} = \delta_{lp} - \tau/k \,, \\
\tau &= k(\delta_{lp} - \delta) \,,
\end{aligned}
\tag{4}
$$

where δ_{lp} is the measured "load-point" displacement (in our simulations the displacement of the end of the spring not attached to the upper plate), τ the spring force divided by the nominal sample surface area (6 cm × 6 cm), and k the elastic stiffness of the combined testing apparatus plus sample between the measurement points. In our numerical simulations this stiffness is given by the effective stiffness of two springs in series,

$$
k_{\text{eff}} = \frac{k_{sp} k_H}{k_{sp} + k_H}
\tag{5}
$$

where k_{sp} and k_H are the spring and gouge stiffness, respectively (H is the gouge thickness). The shear modulus of the gouge layer can be estimated from the initially linear (assumed to be elastic) portion of the loading stress-strain curve at the start of a steady-sliding test. In Fig. B1 of Ferdowsi and Rubin (2020), we show the sensitivity of the gouge shear modulus to hold time duration in SHS tests, and we find that at 5 MPa $G_H \approx 270 - 310$ MPa regardless of hold time. From the value of shear modulus $G_H \approx 300$ MPa, the stiffness k_H can be determined as $k_H = G_H/H = 7.3 \times 10^9$ Pa/m, where $H = 0.04$ m is the gouge thickness. We can further determine k_{sp} in Pa/m from the spring stiffness input, k_{pull}, in LAMMPS in units of N/m, by dividing k_{pull} by the sample surface area. The pulling spring stiffnesses of $k_{pull} = 1 \times 10^{10}, 8 \times 10^5, 2.7 \times 10^4$ N/m then correspond to dimensionless system stiffness $\bar{k}_d \equiv k_{\text{eff}} D_c/(b\sigma) \approx 425$, 12, 0.4, respectively, where the "$\approx$" sign indicates that the values of the normalizing constants b and D_c, determined from fitting simulated velocity-step tests, are known only to within about 10%. The dimensionless stiffness $\bar{k}_d \approx 425$ represents the approximate upper bound for what we can achieve; $k_{pull} = 10^{10}$ N/m is large enough that essentially all the elastic compliance comes from the gouge. The dimensionless system stiffnesses of $\bar{k}_d \approx 12$ and 0.4 were chosen to be close to the values of $\bar{k}$ in the SHS experiments performed on the Tullis rotary shear apparatus at Brown University (Beeler et al., 1994), to which we compare some of our granular model observations. After performing the granular simulations reported in this work, our estimates of $\bar{k}_d$ for the lab data were reduced by 1/3 from their inital values, to $\bar{k}_d \approx 8$ and 0.27. For analysis of our simulation data we used values of $D_c = 1.77 D_{mean} = 0.0053$ m, $a = 0.0247$, and $b = 0.0178$ which were obtained from velocity-stepping simulations (Ferdowsi & Rubin, 2020).

The simulations reported here were performed primarily with two initial steady-state load-point velocities of $V_i = 2 \times 10^{-2}$ and 10^{-1} m/s, and in most simulations we used a reslide velocity equal to the initial velocity. However, in a small number of cases we changed the reslide velocity to search for deviations from the predictions of existing RSF equations; any such deviations would be relevant to models of earthquake nucleation. We also performed a series of slide-hold simulations at the smaller sliding velocity of $V_i = 2 \times 10^{-4}$ m/s. In laboratory experiments, the sliding velocity is typically on the order of 1 μm/s; however, running simulations at such velocities is not yet possible with the DEM method within reasonable computational costs. Our velocities still correspond to the quasi-static regime of shearing (Ferdowsi & Rubin, 2020). In the simulations described here, reducing the grain size and model dimensions by the same factor, while keeping V_i the same, results in simulations that are dimensionally identical (except for the effect of gravity, which is active but insignificant in our model) (See Appendix A in Ferdowsi and Rubin (2020) for details). The majority of the simulations were performed with a very high restitution coefficient of $\epsilon_n = 0.98$, such that the system is damped minimally. However, we also have run a series of slide-hold simulations with a much lower restitution coefficient of $\epsilon_n = 0.3$.

4 Results and discussion

4.1 Slide-hold simulations

In this section we present the slide-hold (SH) behavior of the granular model. Since individual simulations tend to be somewhat noisy, all simulation signals presented in this manuscript are averaged over eight different realizations (initial grain arrangements) of the model, all subjected to the same boundary conditions. We define friction as the ratio of shear to normal stress τ/σ, with τ and σ defined as the shear and normal force per unit area exerted by the gouge particles on the upper (driving) plate. This definition ensures that we are measuring the frictional strength of the gouge at the boundary with the upper plate, should that differ from the applied spring force (any mismatch leading to acceleration of the upper plate). In the absence of significant accelerations that are coherent when averaged over $x-y$ planes, from force balance the shear stress as we have defined it is uniform throughout the gouge.

Figures 2a-b show the variation of normalized friction with normalized hold time for SH tests, with initial sliding velocities of $V_i = 2 \times 10^{-2}$ and 10^{-1} m/s shown by the blue and black curves, respectively. Panel (a) shows the results of simulations run with system stiffnesses $\bar{k}_d \approx 425$ and 0.4 (solid and dashed lines, respectively), while panel (b) shows simulations with system stiffness $\bar{k}_d \approx 12$ (panels (a) and (b) have been separated only for clarity). Lowering the stiffness delays the onset of stress decay because a given stress reduction then requires a longer slip distance; at constant sliding velocity, elasticity dictates that the normalized stress change $\Delta\tau/b\sigma$ reaches -1 when $t_{hold}/(D_c/V_i) = \bar{k}^{-1}$, which is roughly when the stress trajectories in Figure 2 leave their initial plateau. From dimensional analysis, standard RSF (equations 1–3 with constant parameter values) predicts that the curves for the same $\bar{k}$ but different V_i overlap identically when plotted versus dimensionless hold time $\bar{t}_{hold} \equiv t_{hold}/(D_c/V_i)$. Our simulations at the two sliding velocities with $\bar{k}_d \approx 425$ show a stress decay response that is not exactly the same, but they are nevertheless similar to each other within their standard deviations. The stress decay response for the two velocities differ more significantly at the lower stiffnesses of $\bar{k}_d \approx 0.4$ and 12.

Figures 2a & b also include the predictions of the Aging and Slip laws for the stiffnesses used in the granular model. These predictions are obtained using the RSF parameter values determined independently from Slip law fits to simulated velocity steps performed on the identical granular system (Ferdowsi & Rubin, 2020). For $\bar{k}_d \approx 425$, the stress decay of the granular model is in excellent agreement with the Slip law prediction. There is also reasonable agreement for the lower stiffnesses of $\bar{k}_d \approx 0.4$ and 12, where the Slip law prediction generally lies between the curves for the different V_i. In contrast, for the two larger stiffnesses the Aging-law prediction significantly underestimates the stress decay at long hold times. The shallowing slope of the stress decay for the Aging law results from its prediction of continual state evolution, $\dot{\theta} \approx 1$ in equation 2, even at vanishing slip rates. For $\bar{k}_d = 0.4$, the Aging and Slip law predictions are almost indistinguishable.
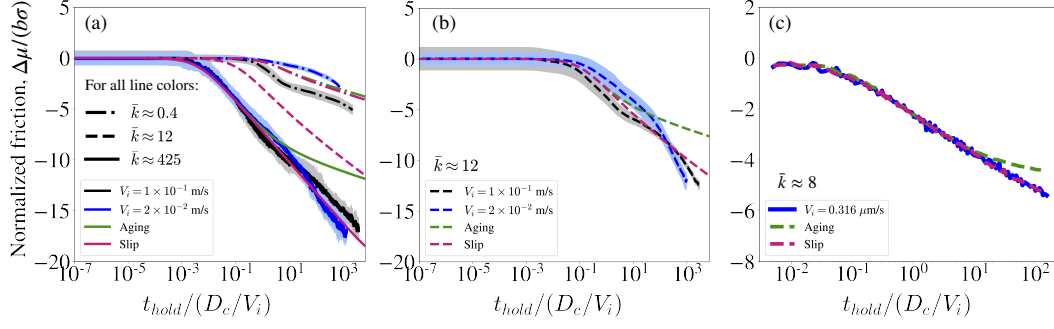
Figure 2. The slide-hold behavior: The blue and black lines in panels (a) & (b) show the variation of friction coefficient, normalized by the RSF parameter b, as a function of normalized hold time, for granular slide-hold simulations with prior sliding velocities V_i of 2×10^{-2} (blue) and 10^{-1} (black) m/s. Panel (a) shows the behavior of the systems with stiffness $\bar{k}_d \approx 425$ and 0.4, while panel (b) shows the behavior of the system with stiffness $\bar{k}_d \approx 12$. The pink and green lines in panels (a) & (b) further show the predictions of the Slip and Aging laws, respectively, using the RSF parameters ($D_c = 0.0053$ m, $a = 0.0247$, $b = 0.0178$) determined independently from Slip-law fits to velocity-step tests performed on the same model (Ferdowsi & Rubin, 2020). The predictions of the Slip and Aging laws are shown with different line styles for different system stiffnesses (the Slip law prediction for $\bar{k} = 12$ is included in panel (a) only for reference). Granular simulation results in panels (a) & (b) are averaged over 8 different realizations (initial grain arrangements) subjected to the same imposed loading conditions. Black and blue lines show the mean behavior of the realizations for each system, and the width of the gray and blue shades around each line shows the 2-sigma deviations. The confining pressure in all simulations is 5 MPa. (c) The blue line shows the variation of friction coefficient, normalized by the RSF parameter b, as a function of normalized hold time, for an experiment performed in the Tullis rotary shear apparatus at Brown University on a granite sample with prior sliding velocity $V_i = 0.316$ μm/s. The system stiffness for this experiment is $\bar{k}_d \approx 8$, and the confining stress is 25 MPa. As in panels (a) and (b), the pink and green lines show predictions of the Slip and Aging laws, respectively, using the RSF parameters ($D_c = 2$ μm, $a = 0.013$, $b = 0.016$) obtained from Slip-law fits to velocity-step tests on the same experimental sample. We used the same RSF parameters to calculate the dimensionless stiffness $\bar{k}$ for the lab data.

This can be rationalized by noting that for this low stiffness and the hold times reached in these simulations, the interface never gets far below steady state, and in the vicinity of steady state the Aging and Slip laws are asymptotically identical.

An example of frictional behavior during a laboratory slide-hold experiment on rock is shown in Fig. 2c. The experiment was performed with the Tullis rotary shear apparatus at Brown University, on a granite sample with initial sliding velocity $V_i = 0.316$ μm/s, system stiffness $\bar{k}_d \approx 8$, and confining stress 25 MPa. The Aging and Slip law predictions for the experiment are also shown with green and pink lines, respectively. These predictions, similar to the RSF predictions for the granular model, are obtained using the RSF parameter values determined independently from Slip law fits to the experimental velocity-stepping tests on the same sample. Overall, as with the fits to the granular simulations, they indicate that the Aging law underestimates the stress decay in the lab at long hold times, while the Slip law provides a very good prediction of the behavior. Similar results were obtained from the laboratory slide-hold data of Beeler et al. (1994) analyzed by Bhattacharya et al. (2017), although in that case the constrained Slip law fit to the hold data was not as good as that in Figure 2c (in this case only $a - b$ was constrained by velocity steps on the same sample). Comparing the behavior of both the lab data and the granular model to the Aging and Slip law predictions, especially Figures 2b and c with close to the same stiffness, we conclude that although

the stress decay in the simulations is not strictly log-linear as for the lab data, the granular model qualitatively captures the stress decay observed in laboratory slide-hold tests.
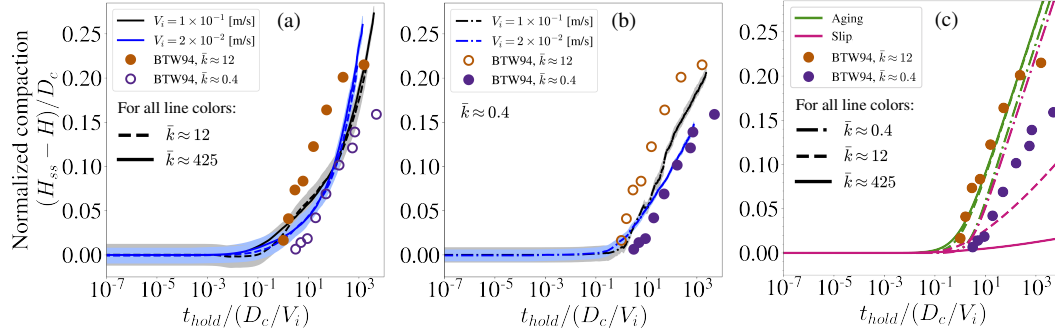

Figure 3. Gouge compaction during slide-holds: The blue and black lines in panels (a) & (b) show the variation of gouge compaction, normalized by the RSF characteristic slip distance D_c, as a function of normalized hold time, for granular slide-hold simulations with prior driving velocities V_i of 2×10^{-2} (blue) and 10^{-1} (black) m/s. Panel (a) shows the behavior for stiffnesses $\bar{k}_d \approx 425$ and 12, while panel (b) shows the behavior of stiffness $\bar{k}_d \approx 0.4$. The widths of the gray and blue shades around the mean behavior lines indicate 2-sigma deviations. (c) The pink and green lines show the evolution of log(state) under the Slip and Aging laws, respectively, using the RSF parameters that are determined independently from Slip-law fits to velocity-step simulations (Ferdowsi & Rubin, 2020). The state evolutions are scaled by an arbitrary factor $\beta = 0.0377$ to match the lab compaction data. Different line styles correspond to different system stiffnesses as described in the legend. The filled and empty dots in all panels show the change in gouge thickness during hold experiments on a granite sample reported by Beeler et al. (1994), who used two different ($\bar{k}_d \approx 8$ and 0.27) machine stiffnesses. The dots are filled or empty in panels (a) and (b) depending on the machine stiffness that is most appropriate to compare the granular model behavior to in that panel. An estimated slip-weakening distance $D_c \approx 2\mu$m is used to normalize compaction data in laboratory experiments. The lab experiments with stiffness $\bar{k}_d \approx 0.27$ and 8 were performed with sliding velocities $V_i = 1$ μm/s and 0.32 μm/s, respectively. Both low and high stiffness laboratory experiments were performed at 25 MPa confining pressure.

The stress decay during slide-holds clearly rules out the Aging law for the evolution of state in both the granular model and laboratory experiments. This is despite the fact that log-time fault-normal compaction is almost universally observed during laboratory holds. This compaction is thought to be consistent with an Aging law-like evolution of state; that is, in theoretical justifications of the Aging law, the same mushrooming of highly-stressed contacts that is considered to be responsible for log-time increase of true contact area and frictional strength, would also lead to log-time compaction (Berthoud et al., 1999; Sleep, 2006). The same argument would suggest that if the stress data during holds is well modeled by the Slip law, with its relative lack of state evolution, the fault-normal compaction would be much less. This potential conflict between the stress and fault-normal displacement data from laboratory holds was noted previously by Bhattacharya et al. (2017).

In our previous work, we observed that in addition to matching the stress decay during laboratory holds, the granular model led to log-time reduction in gouge thickness for $\bar{k}_d \approx 425$ (Ferdowsi & Rubin, 2020). Here we examine the changes in gouge thickness during slide-holds using stiffnesses more appropriate for lab experiments. Figure 3a shows the gouge compaction with hold time in the granular model with stiffnesses $\bar{k}_d \approx 425$ and 12, in comparison to the gouge compaction observed in the laboratory for two system stiffnesses $\bar{k}_d \approx 8$ (filled circles) and 0.27 (lab data from Beeler et al. (1994), as reported by Bhattacharya et al. (2017). This plot indicates that the magnitude of gouge compaction in the granular model is in general agreement with laboratory observations,

after both are normalized by their appropriate value of D_c. The gouge compaction in the granular model with the lower stiffness $\bar{k}_d \approx 0.4$ is shown separately in Fig. 3b for clarity, where now the lab data for $\bar{k}_d \approx 0.4$ are shown as filled circles. Together, panels (a) and (b) show that gouge compaction in the granular model is not strongly dependent on system stiffness, and that the normalized rate of compaction with log time is close to that of the lab data (most obviously for the simulation with lowest stiffness, panel (b), which is the simulation for which the compaction is most nearly log-linear). However, the lab data show more of a stiffness-dependent offset along the time axis than do the simulations.

The weak dependence of the compaction rate on stiffness in the granular simulations contrasts with the strong dependence of the stress decay rate in the same simulations (Fig. 2). Fig. 3c shows the evolution of log(state) as predicted using the RSF Aging and Slip laws for the three stiffnesses used in the granular model, scaled by an arbitrary factor $\beta = 0.0377$. State evolution under the Aging law is largely independent of stiffness (because except for the very earliest hold times, $\dot{\theta} \approx 1$) In this the Aging-law prediction resembles the compaction behavior observed in both the lab and in the granular model. The evolution of state under the Slip law for the lowest stiffness $\bar{k}_d \approx 0.4$ is again very similar to that for the Aging law. However, as the system stiffness increases, the evolution of state under the Slip law significantly decreases because the amount of slip decreases. Translating this state evolution to fault-normal compaction as in Figure 3c, the prediction would be that compaction for the Slip law should be strongly stiffness-dependent, completely unlike compaction in the simulations and the lab data (Figures 3a and b). This happens at the same time that the Slip law matches the stress decay in the model (and lab experiments) quite well.

4.2 Slide-hold-reslide simulations

We have thus far presented a detailed comparison of the slide-hold behavior of the granular model to both lab data and the RSF Aging and Slip laws. A main motivation for conducting SHS experiments in rock friction laboratories is to better understand the fault healing that occurs during interseismic intervals, healing that is necessary for repeated earthquakes to occur on the same section of fault. This healing historically has been measured by the peak stress $\Delta\mu_{peak}$ upon resliding following a hold (see the inset in Figure 4a), under the assumption that little state evolution occurs in the short time or slip distance between the start of the reslide and the peak stress. Because the Aging law embodies fault healing (state evolution) with time even in the absence of slip, for the same parameter values it generates more healing during holds than the Slip law. More diagnostically, sufficiently long hold times lead to $V\theta/D_c \ll 1$, so from equation 2 for the Aging law, $\dot{\theta} \approx 1$. This means that for long hold times the rate of healing with log hold time is independent of how much slip accumulates during the hold, and hence it is independent of the elastic stiffness of the loading system (Beeler et al., 1994; Bhattacharya et al., 2017). These authors further showed that the Aging law predicts that the reduction in log(state) between the start of the reslide and peak stress is independent of hold duration, and hence that the predicted change in peak friction with log hold time, $d\Delta\mu_{peak}/d\ln(t_{hold})$, equals the RSF parameter b (equation (1); note that at peak stress $d\tau/dt = 0$ so from elasticity the sliding velocity equals the load-point velocity). This property was exploited by Beeler et al. (1994), who ran lab experiments with two loading machine stiffnesses and found that, indeed, for long hold times, the rate of healing was independent of stiffness. Bhattacharya et al. (2017) later showed that, for the two stiffnesses and hold durations of those experiments, the same stiffness-independent rate of healing could be achieved by the Slip law, but over a more restricted range of RSF parameters. Those parameters do not include the ratio of a/b appropriate for our granular simulations.

Before proceeding to the results of the granular slide-hold-reslide simulations, it is worth considering what it means to compare those results to laboratory experiments. The ratio a/b for the granular simulations, determined from simulated velocity steps, is ~1.4, and may be fixed by our choice of spherical particles, the particular grain size distribution, and the tangential and normal contact laws we have adopted (Ferdowsi & Rubin, 2020). This value of a/b is slightly high by lab standards, and we are not aware of lab experiments that push surfaces with such values far enough from steady state to be useful for constraining models of state evolution. Therefore we do not neces-
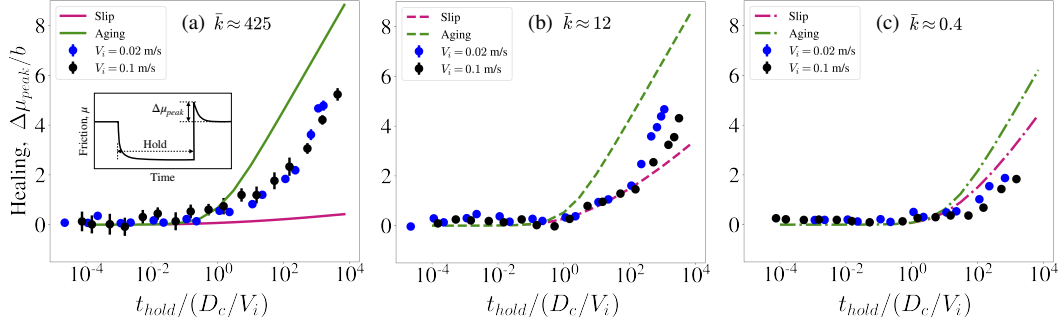
Figure 4. Frictional healing in the granular model: Solid circles show $\Delta\mu_{peak}$ normalized by the RSF parameter b (estimated from velocity steps), as a function of normalized hold time in granular slide-hold-slide simulations at $V_i = 2 \times 10^{-2}$ and 1×10^{-1} m/s. Panels (a), (b), and (c) show the results for system stiffnesses of $\bar{k}_d \approx 425$, 12, and 0.4, respectively. Error bars are 2-sigma deviations of 8 different realizations. The green and pink lines in each panel show the predictions of the Aging and Slip laws, respectively, for that specific system stiffness using the RSF parameters obtained from velocity-step tests. The inset in panel (a) shows the schematic of a slide-hold-slide test and the definition of frictional healing, $\Delta\mu_{peak}$.

sarily expect our granular simulations to match any particular lab experiment. Nonetheless, we were able to claim that the simulations successfully capture the phenomenology of laboratory velocity-step experiments. For velocity steps, this phenomenology entails that the amplitudes of the changes in friction with velocity and state evolution are proportional to the logarithm of the velocity step (in RSF these amplitudes are controlled by the magnitudes of the parameters a and b), and that friction evolves to its future steady state value over a characteristic slip distance, independent of the size or sign of the velocity step. As a corollary, because these same attributes of velocity-step experiments are well-captured by the Slip law for state evolution, we were able to find parameter values for the Slip version of the RSF equations that matched the granular simulations. A similar approach allowed us to make the claim that the granular simulations also captured the phenomenology of laboratory slide-hold protocols – that is, for both the granular simulations and lab experiments, the Slip-law parameters determined from velocity steps did a reasonable job matching the stress decay during holds (Figure 2), even though the values of the RSF parameters used to match the simulations and the lab experiments were not the same.

Because neither the Aging law nor the Slip law successfully models laboratory reslide data using parameters constrained by other protocols (either velocity steps or the hold portions of slide-hold-reslides), a similar approach for comparing the granular simulations to laboratory reslide data is not available to us. Instead, we are limited to trying to reproduce the phenomenology of the reslide experiments, which can be summarized as follows. It is well established that the peak friction upon resliding increases approximately linearly with log hold time (J. H. Dieterich, 1972; Beeler et al., 1994; Baumberger & Caroli, 2006; Marone & Saffer, 2015). The slope of this increase, $d\Delta\mu_p/d\ln(t_{hold})$, is plausibly equal to b, as predicted by the Aging law, but in fact we are unaware of any SHS experiments in which the value of b was determined independently on the same sample (e.g., from velocity steps) These slopes vary from a maximum of ~0.01 for granite in the study of Beeler et al. (1994), similar to the expected value of b, to a minimum of ~0.0035, plus or minus several tens of percent depending upon V_i, in the study of Marone and Saffer (2015), a value that seems lower than typical estimates of b by a factor of 2–3.

Beyond this, results seem to be limited to single studies. As mentioned previously, Beeler et al. (1994) showed that the rate of frictional strengthening $d\Delta\mu_p/d\ln(t_{hold})$ was independent of system stiffness, and interpreted this as suggesting that frictional healing depends upon time rather than slip. Marone and Saffer (2015) showed that the rate of frictional strengthening depended upon

V_i, indicative of a velocity-dependence of the RSF parameters or a characteristic velocity in the governing equations not captured by the standard RSF equations (1)–(3).
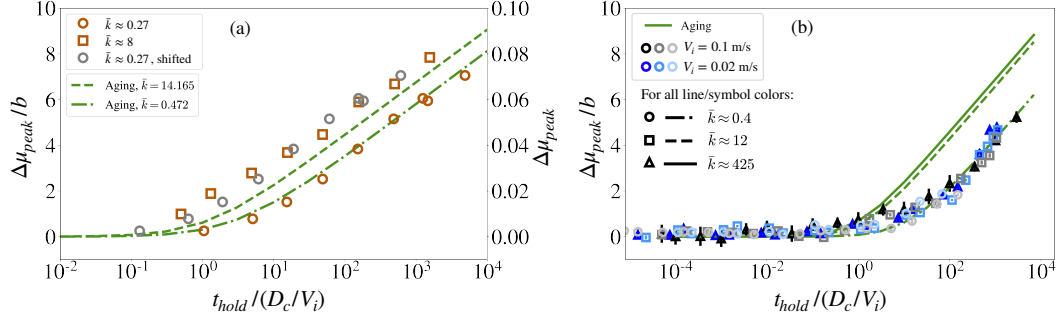

Figure 5. (a) Frictional healing in the lab: Solid circles show $\Delta\mu_{peak}$ as a function of normalized hold time, in slide-hold-slide experiments performed on a granite sample at 25 MPa confining pressure (Beeler et al., 1994) with machine stiffness $\bar{k}_d \approx 0.27$ and 8, at sliding velocities of $V_i = 1$ μm/s and 0.32 μm/s, respectively. The green dashed lines show the evolution of frictional healing, $\Delta\mu_{peak}$, normalized by the RSF parameter $b = 0.0109$ (estimated from the slope of healing vs. time data in this figure) with $a - b = -0.0027$ (Bhattacharya et al., 2017) and $D_c = 2$ μm. These parameters result in normalized stiffness values of $\bar{k}_d \approx 0.472$ and 14.165 used in the Aging law predictions in this plot. (b) The green lines show the predictions of the Aging law for the RSF parameters of the granular model and the three normalized stiffnesses used; note that, as in (a), all the Aging law predictions asymptote to the same slope for large t_{hold}. The data points with shades of gray and blue show the frictional healing in the granular model, $\Delta\mu_{peak}$, normalized by the RSF parameter $b = 0.0185$, versus normalized hold time for the three stiffnesses shown in Figs. 4a-c. The granular model data are shifted horizontally for all stiffnesses and velocities, except for $\bar{k}_d \approx 12$ at velocity $V_i = 0.02$ m/s, to produce a reasonable collapse of the data.

Here we present results of granular SHS simulations for a wide range of hold times at $V_i = 2 \times 10^{-2}$ and 10^{-1} m/s. Panels (a), (b) and (c) in Fig. 4 show the changes in peak stress with hold time for simulations performed with stiffnesses $\bar{k}_d \approx 425$, 12, and 0.4, respectively. The simulations with the highest stiffness produce the most frictional healing over the range of $\bar{t}_{hold}$ we could achieve. Figure 4a shows that for the longest holds, the peak stress increases nearly logarithmically with hold time, in qualitative agreement with laboratory rock friction data. Furthermore, the slope of this increase is very nearly equal to the independently-determined value of b, which as noted above is at least approximately the case for laboratory experiments. In Fig. 4a this is shown by the parallelism between the granular simulation results and the prediction of the Aging law, shown by the green curve, which has the slope b for large hold times (when plotted vs. $\ln[\bar{t}_{hold}]$). The value of b used for the Aging prediction was determined from fits to simulated velocity steps (note that because this value depends only upon the total change in friction from the peak value following a velocity increase to the future steady state value, it is determined independently of any state evolution law; the state evolution laws control the rate of approach to steady state and hence D_c). However, unlike the lab data of Marone and Saffer (2015), there does not appear to be a significant dependence upon V_i, most obviously for the highest-stiffness simulations that have healed the most. Future experiments and simulations that explore a broader range of rate-state parameters, system stiffnesses, and sliding velocities might better illuminate whether there is velocity-dependence in a broad area of parameter space, and the potential origins of such dependence.

Frictional healing in the lowest-stiffness system ($\bar{k}_d \approx 0.4$) has not progressed as far. However, the behavior of all three systems suggest that they may follow the same frictional healing path, just to different extents. This is shown in Figure 5b, where we plot the data for all three stiffnesses, after shifting them along the horizontal axis by an amount that makes the data nearly collapse onto the

data for $V_i = 0.02$ m/s and $\bar{k}_d \approx 12$. Note that the data for $\bar{k}_d \approx 425$ and $\bar{k}_d \approx 12$ in Figure 4 show something of a break in slope at $\bar{t}_{hold} \sim 10^2$, but for $\bar{k}_d \approx 0.4$ this behavior has not yet begun. In this interpretation the data share with laboratory rock friction data (Fig. 5a) the feature that the healing is independent of system stiffness, except for a shift along the $\bar{t}_{hold}$ axis. The predictions of the Aging and Slip laws for the three stiffnesses are further shown in Fig. 4, panels a-c. They demonstrate that the Slip law evolution of state produces a strongly stiffness-dependent frictional healing, while the Aging law produces a healing curve with a stiffness-independent slope, consistent with lab data (Beeler et al., 1994). The $\log(t_{hold})$ shift required to align the data seems to be different for the granular simulations and the lab data, however. For the simulations, healing seems to lag the Aging law predictions (green lines in Figure 4) by roughly the same distance on the log(time) axis at each stiffness, whereas the lab data seem to be consistent with the Aging law prediction for the lower stiffness system, but exceed the predicted healing for the high stiffness system (Figure 5a).

In comparing the granular models to the predictions of the Aging and Slip laws in Fig. 4, we also observe that the healing in the granular model is less than that predicted by the Aging law for all stiffnesses (using RSF parameters obtained from Slip law fits to model velocity-step simulations). The healing in the model is more than that predicted by the Slip law for $\bar{k}_d \approx 425$ and 12, but less than predicted for $\bar{k}_d \approx 0.4$. Thus, the observation of Ferdowsi and Rubin (2020) that for $\bar{k} \approx 425$ the healing in the granular model lies between the Aging and Slip law predictions is not generalizable to all stiffnesses.
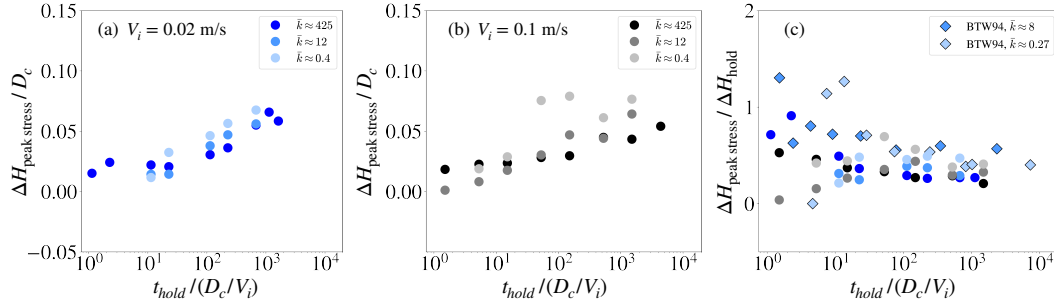

Figure 6. The variation of normalized dilation at peak stress ($\Delta H_{\text{peak stress}} / D_c$) versus hold time, following reslides for the granular model with sliding velocities of (a) $V_i = 0.02$ m/s and (b) $V_i = 0.1$ m/s. The amount of dilation is defined as the change in gouge thickness between the end of the hold and the moment of peak stress, as in Fig. B1 of Bhattacharya et al. (2017). The simulations are performed at three different stiffnesses and 5 MPa confining stress. (c) The ratio of dilation at peak stress ($\Delta H_{\text{peak stress}}$) to compaction at the end of the respective slide-hold in the granular model (circles) and in the lab (diamonds) (data of Beeler et al. (1994), as reported by Bhattacharya et al. (2017)).

In laboratory slide-hold-slide experiments, the reslide portion is accompanied by dilation of the gouge layer, dilation that continues monotonically beyond the moment of peak stress to the future steady-state thickness. We observe the same behavior in our simulations with stiffnesses $\bar{k}_d \approx 425$ and ≈ 12. However, the simulations with stiffness $\bar{k}_d \approx 0.4$ show dilation past the moment of peak stress followed by compaction at larger sliding distances; that is, a non-monotonic approach to the future steady-state value (the steady-state thickness of the simulations at a given sliding velocity are independent of the system stiffness). Figure 6a & b show the variation of dilation at peak stress upon reslides in the granular model for the sliding velocities $V_i = 0.02$ m/s and $V_i = 0.1$ m/s, respectively. We observe that this dilation increases nearly linearly with log-hold time. We further normalize the dilation by the amount of compaction at the end of the respective slide-holds. The ratio of dilation/compaction that results from this analysis is shown in Fig. 6c, and it is plotted alongside the same quantity observed in the lab data of Beeler et al. (1994). Comparing the lab data to the simulations conducted at roughly the same stiffnesses, we find that the relative slopes of the

log-linear portion of the dilation and compaction in both the simulations and lab are in the range $\sim 0.4 - 0.5$, and are there therefore in qualitative agreement with each other.
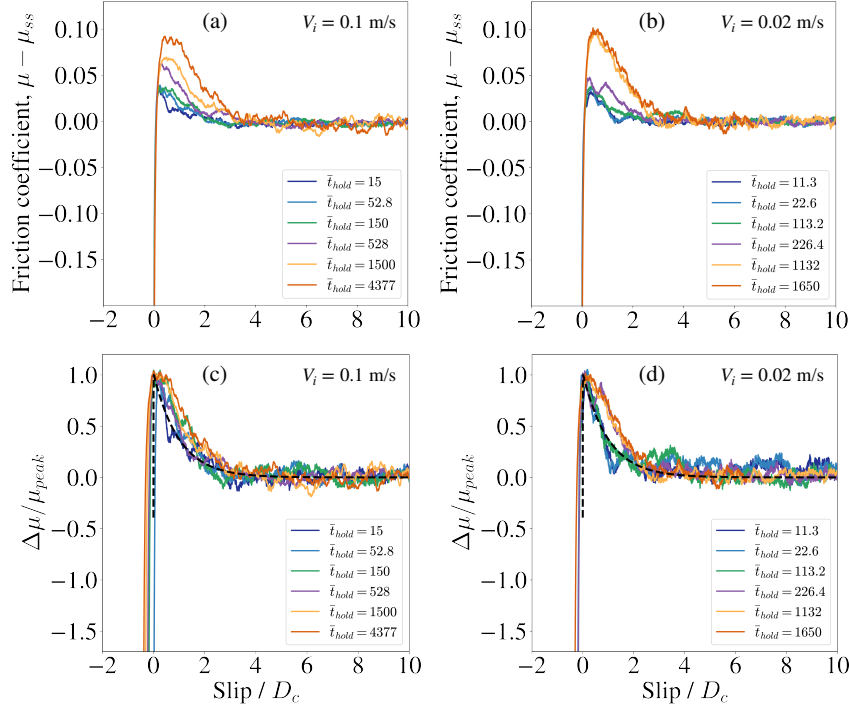

Figure 7. The variation of friction ($\mu - \mu_{ss}$) versus slip distance (Slip / D_c) during the reslide portion of slide-hold-slide simulations, for different values of normalized hold time $t_{hold}/(D_c/V_i)$ and sliding velocities of (a) $V_i = 0.1$ m/s and (b) $V_i = 0.02$ m/s. Panels (c) and (d) show the signals in panels (a) and (b) with values normalized by the peak friction value in each simulation. All simulations are performed with stiffness $\bar{k}_d \approx 425$ at 5 MPa confining stress. The black dashed line in panels (c) and (d) show the Slip law predictions for a one order of magnitude velocity-step increase, using the RSF parameters that provide good fits to velocity steps of various sizes performed with the granular model (Ferdowsi & Rubin, 2020). The Slip law prediction is scaled to the same peak-residual scale as the granular simulation data in the panels. The lines are added to show that the slip-weakening distance D_c increases with hold duration from a minimum value that is consistent with the value appropriate for velocity steps.

Among other features observed in slide-hold-slide tests, Figure 5 of Marone and Saffer (2015) suggests that the slip-weakening distance following the peak stress upon resliding increases with hold duration. This feature is inconsistent with the Slip law prediction, but we see evidence of similar behavior in our granular slide-hold-slide simulations. Figures 7a & b show the variation of friction coefficient with sliding distance in the reslide portion of slide-hold-slide simulations performed after a range of hold times, at two sliding velocities $V_i = 0.1$ and 0.02 m/s, referenced to the steady-state friction value at V_i. These signals show (more obviously in Fig. 7a) that the slip distance to peak friction increases with increasing hold time, as for the Marone and Saffer (2015) data (their Figure 12). Panels c-d in Fig. 7 also include the Slip law prediction for a one-order velocity-step increase, normalized to the same peak-residual value as the reslide friction signals. These two panels more clearly demonstrate the increase in weakening distance with hold time. The reslides at shorter holds have a weakening distance, D_c, roughly equal to the distance observed in the velocity-steps. At longer hold times, D_c further increases, although the amount of increase in D_c in the granular model appears to be less than that observed in the lab data.

In our SHS simulations, we have also investigated whether changing the re-sliding velocity changes either the peak friction or the approach to the future steady-state friction. Any behavior that deviates from the RSF prediction is relevant to models of earthquake nucleation, as the perimeter of an expanding nucleation zone subjects regions that have not slipped for a long time (as in a hold) to successively larger velocity jumps (Ampuero & Rubin, 2008). For this purpose, we have run reslide simulations after a hold time $\bar{t}_{hold} \sim 1650$, with the initial sliding velocity $V_i = 0.02$ m/s and reslide velocities V_r of 0.02, 0.05, 0.1, and 0.3 m/s. In a sense these are velocity-step tests, but run from a single value of state that is much larger than the steady-state value at velocity V_i. The results are shown in supplementary Fig. S2a, where friction is plotted relative to its future steady-state value. The prediction of equation (1), assuming that the change in state between the end of the hold and peak stress is either small or independent of the reslide velocity, is that the difference in $\Delta\mu_{peak}$ between two reslide velocities V_2 and V_1 is equal to $b \ln(V_2/V_1)$. The inset in Fig. S2-a shows that this is very nearly the case, with $\Delta\mu_{peak}$ increasing linearly with $\ln(V_r/V_i)$ with a slope of 0.0155, or 87% of the value $b = 0.0178$ measured in velocity-steps. Furthermore, scaling the $\Delta\mu$ curves by the value $[C + \ln(V_r/V_i)]$ in Fig. S2-b, with the value of $C = 5$ determined empirically (the value of $\Delta\mu_{peak}/b$ determined for $V_r = V_i$), collapses the frictional response for all the reslide velocities onto a single curve, consistent with the Slip law prediction. In other words, within the range of velocities that we have explored, changing the reslide velocity does not affect the weakening distance D_c in the granular model, consistent with the Slip law prediction, and changes the peak friction in accordance with standard RSF.

5 Energetics of granular slide-holds

Although the exact definition of an effective thermodynamic temperature for granular materials is still a matter of much debate (Ono et al., 2002; Blumenfeld & Edwards, 2009; Puckett & Daniels, 2013; Bi et al., 2015; D. Richard et al., 2021), recent research results suggest that the fluctuating kinetic energy in these systems can play a role similar to the effective temperature. For this reason, the fluctuating kinetic energy in granular systems (that is, the kinetic energy determined after subtracting from the velocity vector of each grain the average velocity vector of all the grains in its immediate environment) is often referred to as the "granular temperature", and it has proven to be an important control on the rheological behavior of these systems (Campbell, 1990; Losert et al., 2000; Kim & Kamrin, 2020). In our previous work, we found that the magnitude of the RSF direct effect parameter a in the sheared granular gouge could plausibly be explained as the ratio of the fluctuating kinetic energy to the stored potential energy in the system (Ferdowsi & Rubin, 2020), although this proposal requires further investigation. We further showed that in the quasi-static shearing regime ($V \lesssim 1$ m/s, for a normal stress of 5 MPa), the fluctuating kinetic energy becomes nearly constant, which would suggest a nearly constant magnitude of the direct effect, consistent with most laboratory rock and gouge friction experiments (Kilgore et al., 1993; Bhattacharya et al., 2015). A nearly constant value of effective granular temperature in the quasi-static regime has also been previously reported in experimental granular physics studies (Song et al., 2005; Corwin et al., 2005), although more recent studies of granular systems with different loading geometries (i.e., other than tabular gouge layers between parallel plates) shows that this behavior could be influenced by localized deformation close to driving boundaries (Gaume et al., 2020; Kim & Kamrin, 2020; P. Richard et al., 2020).

In this work, we further examine the evolution of fluctuating kinetic energy in granular slide-hold simulations. The instantaneous per-grain fluctuating kinetic energy is defined in the tensorial form,

$$\boldsymbol{\delta E_k}(t) = \frac{1}{N} \sum_{i=1}^{N} \left[\delta\vec{v}_i(t) \otimes \delta\vec{v}_i(t) + \delta\vec{\omega}_i(t) \otimes \delta\vec{\omega}_i(t) \right], \tag{6}$$

where $\delta\vec{v}_i(t) = \vec{v}_i(t) - \vec{v}_i(z_k, t)$, and $\delta\vec{\omega}_i(t) = \vec{\omega}_i(t) - \vec{\omega}_i(z_k, t)$. In these calculations, $\vec{v}_i(z_k, t)$ and $\vec{\omega}_i(z_k, t)$ are the instantaneous linear and angular velocity fields, respectively, and they are calculated with coarse-graining of the granular model data. The instantaneous linear velocity field is defined as $\vec{v}_i(z_k, t) = (1/N_k) \sum_{i=1}^{N_k} \vec{v}_i(t)$, in which $v_i(t)$ is the linear velocity of the ith particle within the rectangular cuboid with dimensions ($L_x, L_y, \Delta z = 1.37 D_{mean}$), and N_k is the total number of grains
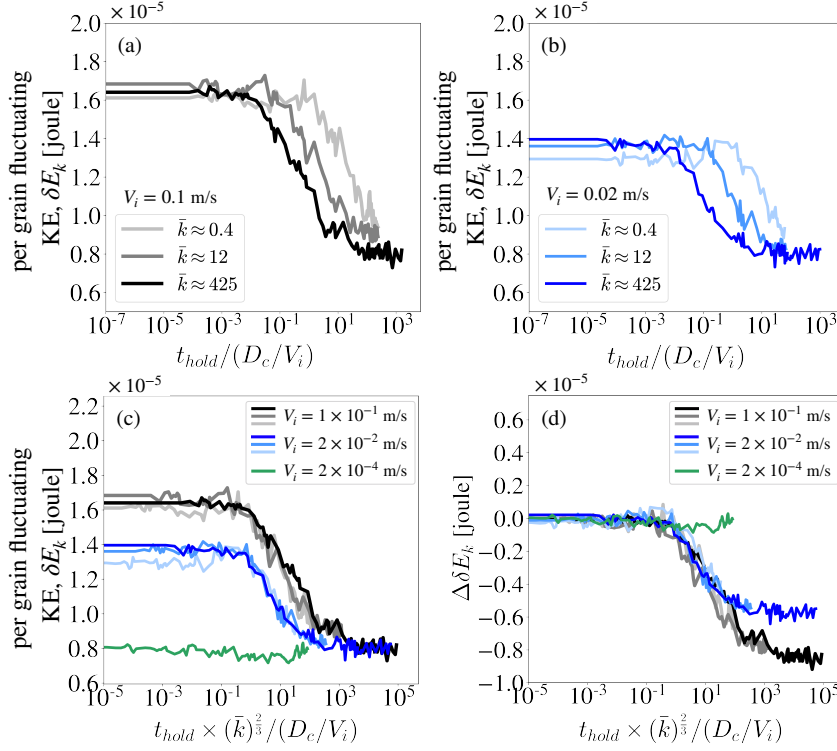
Figure 8. The variation of per grain fluctuating kinetic energy (δE_k) with hold time in slide-hold simulations performed with three system stiffnesses $\bar{k}_d \approx 425$, 12, and 0.4, at two sliding velocities of (a) $V_i = 0.1$ m/s and (b) $V_i = 0.02$ m/s. (c) The variation of δE_k with (hold time)$\times$ (system stiffness, $\bar{k}_d$)$^{\frac{2}{3}}$ for all data shown in panels (a) and (b). (d) same as panel (c) with δE_k referenced to its initial value ($\delta E_{k,0}$) for each simulation. The green lines in panels (c) and (d) show the variation of δE_k and $\delta E_k - \delta E_{k,0}$ for simulations with sliding velocity $V_i = 2 \times 10^{-4}$ m/s and stiffness $\bar{k}_d \approx 425$. All simulations are performed at 5 MPa confining stress.

within each cuboid. The instantaneous angular velocity field is similarly defined as $\vec{\omega}_i(z_k, t) = (1/N_k)\sum_{i=1}^{N_k} \vec{\omega}_i(t)$, where $\vec{\omega}_i(t)$ is the angular velocity of the ith particle.

The variation of per grain fluctuating energy δE_k with hold time for slide-holds with initial sliding velocities $V_i = 0.1$ and 0.02 m/s and three different system stiffnesses are shown in Figs. 8a and 8b, respectively. The curves appear somewhat noisy because the individual data points are snapshots and not averages over some time window. The results show that with these two initial velocities, for moderate hold times δE_k decreases log-linearly over about 4 orders of magnitude in hold time, and then plateaus at roughly 50% of its initial steady-state value. Decreasing the system stiffness delays the onset of the reduction in δE_k, presumably because this allows stresses and sliding velocities near the prior steady state to persist for longer times, but does not otherwise change the shape of the energy reduction curves. This is shown by Fig. 8c, where for both V_i we further multiply the normalized hold time $\bar{t}_{hold}$ by $\bar{k}_d^{2/3}$, resulting in the collapse of all the simulation results for each initial velocity (at this point the choice of 2/3 for the power is strictly empirical). Plotting the change in δE_k from its initial steady state value further shows that the onset of the kinetic energy reduction is similar for both values of V_i (Figure 8d).

Figure 8c also shows that although the curves for the lower V_i have a slightly smaller δE_k at steady state ($\delta E_{k,ss}$), for all stiffnesses both V_i appear to plateau to the same value of δE_k at large hold times. This raises the question of whether there would be any reduction in δE_k during the hold for values of V_i small enough for $\delta E_{k,ss}$ to be at or below this plateau value. Ferdowsi and Rubin (2020) found that the steady-state value of δE_k decreased from about 1.7×10^{-5} J at $V = 10^{-1}$ m/s

to slightly below 10^{-5} J at $V = 10^{-4}$ m/s (triangles in Figure 9b), close to the plateau value of δE_k in Figure 8c. For this reason we ran slide-hold simulations with $V = 2 \times 10^{-4}$ m/s, about the lowest value that could reach moderate values of $\bar{t}_{hold}$ in a reasonable amount of computation time (about 1.5 months). For the same reason the simulations were run only at the largest stiffness; this leads to the largest reduction in δE_k for a given $\bar{t}_{hold}$. We find that, indeed, δE_k for these simulations starts near the plateau value for the larger V_i in Figure 8c, and undergo very little decay during the hold. Despite this, the stress decay, when plotted vs. dimensionless hold time, appears very similar to that for $V_i = 2 \times 10^{-2}$ and 10^{-1} m/s (supplementary Fig. S1). This result raises the possibility that the value of 0.8×10^{-5} J for δE_k represents something of a floor for this granular system, as long as stresses are large enough to drive inelastic deformation. Because of the long computation times required we have been unable to explore this under conditions of steady-state sliding, but for the largest-stiffness holds in Figure 8, the velocities at the end of the simulations were $\sim 10^{-8} - 10^{-7}$ m/s for the different V_i (Fig. 9a). The variation of per grain fluctuation energy versus sliding velocity during holds follows closely the trend we have observed in the steady-state simulations, although it extends that trend to much lower velocities (Fig. 9b), and this suggests the sliding velocity is likely a primary factor in controlling the fluctuating energy, whether or not the system is at quasi-steady state.
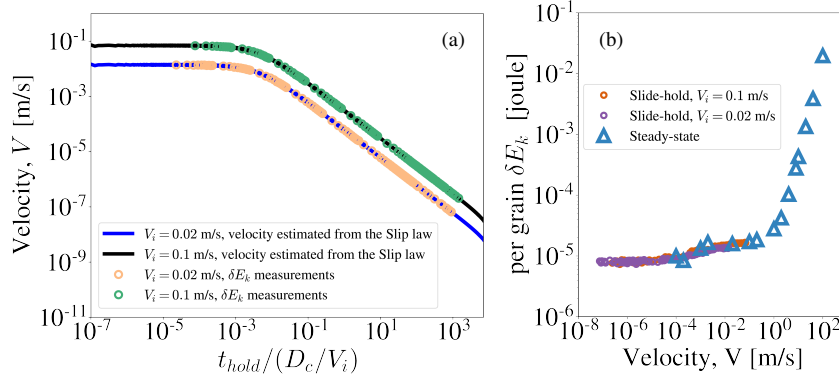

Figure 9. (a) Estimated sliding velocities during the slide-hold simulations with $\bar{k} \approx 425$ and initial sliding velocities $V_i = 0.02$ m/s and 0.1 m/s in Figure 2a (solid lines), and the times at which measurements of the per grain fluctuating kinetic energy (δE_k) were made (open circles), as functions of dimensionless hold time. Determining the slip speed directly from the simulations by taking the time-derivative of equation (4) (with $\delta_{lp} = 0$) results in very noisy velocity histories. Instead, we estimate the slip speed from the Slip law fit to these data. These estimated velocities equal the actual velocities whenever the simulations and the Slip law fit (solid red line in Figure 2a) have the same slope at the same value of t_{hold}. (b) The variation of per grain fluctuating kinetic energy with sliding velocity in the slide-hold simulations of panel (a) (magenta and brown circles) and in steady-state simulations reported in Ferdowsi and Rubin (2020) (blue triangles; the break in slope just below 1 m/s marks the boundary between the quasi-static and inertial regimes of flow). All simulations are performed at 5 MPa confining stress.

We do not yet understand what controls the nearly fixed value of the fluctuating kinetic energy at long hold times or low steady-state sliding speeds in our simulations. For as long as δE_k is nearly constant, the energy loss from grain-grain friction and inelastic collisions must be balanced by work done on the gouge by the moving upper plate (or a reduction in elastic potential energy, but this is not an option during steady sliding, and even during holds, at constant confining pressure this strikes us as a less likely source). During load-point holds this work comes from both shearing (equivalent to the potential energy loss of the attached spring) and compaction. In these high-stiffness simulations the shearing and compaction velocities are of the same order of magnitude. As both decay roughly logarithmically with time during the hold, the rate of energy loss must also decay logarithmically

with time. For our default restitution coefficient ϵ of ~ 0.98, collisions are nearly perfectly elastic and we presume that most of the energy loss is due to grain-grain friction. To explore the effect of increasing the collisional energy loss, we ran simulations with $\epsilon \sim 0.3$, for $\bar{k}_d \approx 12$. The results of these highly damped simulations are shown in Fig. 10. We find that the stress decay is nearly indistinguishable from that with the higher restitution coefficient (Figure 10a), and that while δE_k for the lower restitution coefficient is offset to lower values, the shape of the curve of fluctuating energy with hold time is not much different (Figure 10b). We conclude that within the range explored, the choice of restitution coefficient does not significantly influence the mechanical behavior of these systems at such low strain rates, consistent with previous results (MiDi, 2004; Ferdowsi & Rubin, 2020).
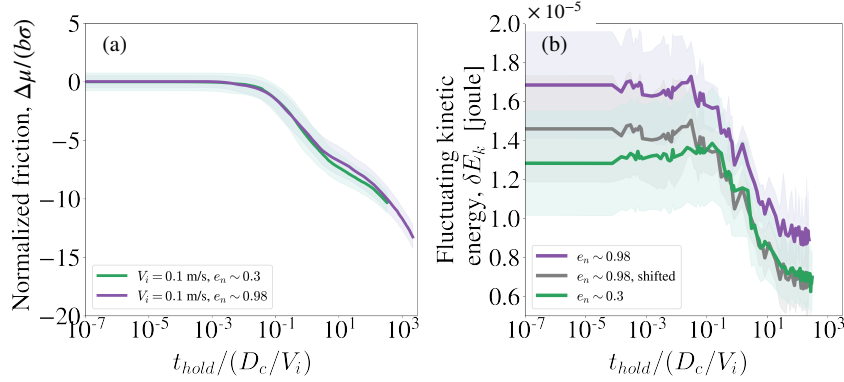

Figure 10. (a) The variation of friction coefficient, normalized by the RSF parameter b, as a function of normalized hold time, for granular slide-hold simulations with sliding velocity 10^{-1} m/s and two restitution coefficients of $\epsilon \sim 0.98$ and $\epsilon \sim 0.3$. (b) The variation of fluctuating kinetic energy with normalized hold time for the simulations in panel (a). The shaded regions indicate 2-σ standard deviations of 8 different realizations. The gray curve shows the fluctuating kinetic energy for the simulation with $\epsilon \sim 0.98$ shifted vertically.

If, as was proposed by Ferdowsi and Rubin (2020), the RSF direct effect parameter a is proportional to δE_k, then Figure 8 suggests that a might vary by a factor of ~ 2 over the duration of the holds with the larger V_i. One could then ask if the generally good fit of the Slip law, using constant parameter values, to the decay of friction during these same holds and to laboratory data, as in Figure 2, is really supportive of the Slip law for state evolution. For example, is it possible that the friction data could be well fit by the Aging law, given the proper velocity-dependence of a? However, we note that for the highest-stiffness simulations in Figures 2 and 8, the continual log-linear stress decay continues to be well fit by the Slip law with constant parameter values even for dimensionless hold times larger than $\sim 10^{0.5}$, where δE_k is essentially constant. In addition, for the simulation with $V_i = 2 \times 10^{-4}$ m/s in supplementary Figure S1, δE_k is roughly constant and t_{hold} is arguably large enough to show that the friction data are more consistent with the Slip law than the Aging law. We leave further investigation of the potential relation between measures of effective temperature and the value of a in granular simulations for future work.

6 Conclusions

In this work, we investigated the behavior of a sheared granular layer subjected to loading conditions designed to mimic laboratory slide-hold-slide experiments, for a range of sliding velocities and system stiffnesses We compared the transient frictional behavior of the model to existing rock friction data, as well as to the predictions of standard rate-state friction (RSF) constitutive equations. For the past few decades it has been common in the rock deformation and earthquake physics communities to interpret the direct rate dependence of RSF as resulting from a thermally-activated process involving the breaking of chemical bonds at contacting asperities, and to interpret state

evolution as due to time-dependent plasticity (or perhaps time-dependent bond strengthening) at those asperities. We have removed this basic ingredient from our simulations, and instead explored whether transient friction as observed in the laboratory could arise simply from momentum transfer in a granular layer with constant friction at grain/grain contacts. Such a granular layer might represent a natural fault gouge, or, in the laboratory context, a synthetic gouge layer, a powder that arises during slip on initially bare rock surfaces, or, owing to similarities in behavior between granular systems and disordered solids (references?), perhaps amorphous wear products on those surfaces. Simulated velocity steps in the same granular model have already shown a direct velocity-dependence and an opposing state evolution-dependence of friction, each proportional to the logarithm of the velocity jump, with magnitudes (the RSF parameters a and b) of ∼0.02, not far from lab values. In addition, state evolution following the velocity jumps occurs over a slip distance that is independent of the size and sign of the velocity step, consistent with laboratory experiments and the Slip law for state evolution. A final motivation for our simulations is that while the RSF equations are largely empirical, the granular model is physics-based, and its output allows us to investigate and perhaps understand why it behaves as it does.

The behavior of the granular flow model in slide-hold (SH) simulations appears to closely resemble laboratory experiments in two important respects. First, the continual stress decay during the hold is reasonably well modeled by the Slip version of the RSF equations, using parameter values determined independently from velocity step tests on the identical system. This is consistent with lab data, as is the result that for both the granular simulations and lab data, the Aging version of the RSF equations predict too little stress decay (too much healing, i.e. state evolution, which for the Aging law progresses with time rather than slip) (Bhattacharya et al., 2017). Under standard RSF, with no intrinsic velocity scale, the stress decay as a function of normalized hold time $t_{hold}/(D_c/V_i)$ must be independent of the initial sliding velocity V_i. This is approximately the case for our stiffest simulations ($\bar{k} \sim 425$), but larger differences arise for the stiffnesses more appropriate for lab experiments ($\bar{k} \sim 12$ and 0.4), where the prediction of the Slip law falls roughly between the simulation results. There is not much lab data investigating this, but the experiments of (Marone & Saffer, 2015) on simulated gouge show a modest dependence on V_i, however, the sign of the dependence seems to be opposite from the granular simulations. The source of the V_i-dependence in the granular simulations, and whether it might be related to the variation of δE_k for $10^{-4} \lesssim V \lesssim 10^{-1}$ m/s in Figure 9b, is unknown.

Second, in both the granular simulations and laboratory experiments, the fault layer undergoes compaction roughly linearly with log time. Even the rates are roughly comparable, at $\sim 0.05D_c$ per decade of hold time in Figure 4. Log-time compaction is consistent with standard interpretations of the time-dependent Aging law for state evolution (compaction being a proxy for growth of true contact area), even though in both the granular simulations and lab experiments the stress decay is consistent with the Slip law and not the Aging law. As with the large velocity-step decreases decribed by Ferdowsi and Rubin (2020), this suggests a decoupling between state evolution and changes in fault or gouge thickness, in both the lab and the granular simulations, that seems inconsistent with traditional interpretations of RSF.

The reslide portion of our granular slide-hold-slide simulations share with laboratory experiments the result that for sufficiently long holds the peak friction upon resliding ("frictional healing", $\Delta\mu_{peak}$) increases nearly linearly with the logarithm of hold time. (J. H. Dieterich, 1972; Marone et al., 1990). This long-term healing rate, $d\Delta\mu_{peak}/d\ln(t_{hold})$, is insensitive to the system stiffness, meaning it is independent of how much slip accumulates during the hold, consistent with laboratory experiments (Beeler et al., 1994). It is also consistent with the Aging law for state evolution but, except over a limited range of parameter space, not the Slip law. In the granular simulations the long-time healing rate is very close the RSF evolution-effect parameter b, as predicted by the Aging law, and as is approximately the case for some but not all laboratory experiments (Beeler et al., 1994; Marone & Saffer, 2015). The granular simulations cannot be fully described by the Aging law, in that the onset of the log-linear healing is delayed to longer hold times in the granular model than in the Aging law prediction, using RSF parameters determined by fitting velocity steps. However, we note that similar mismatches arise between the Aging law and laboratory experiments, even when

b and D_c in the RSF equations are treated as free parameters (e.g., Figure 6a of Bhattacharya et al. (2017), where only $a - b$ is held fixed because that is all that was determined from velocity steps on the same sample in the experiments of Beeler et al. (1994)). Laboratory observations on synthetic gouge samples (Marone & Saffer, 2015) suggest that frictional healing as a function of normalized hold time may be dependent upon V_i, inconsistent with standard RSF with no intrinsic velocity scale. We see a modest V_i-dependence only for our intermediate stiffness of $\bar{k} = 12$.

To summarize, the granular model mimics laboratory slide-hold experiments in that the stress decay during the hold is well approximated by the Slip law for state evolution, using parameter values determined from velocity steps on the same sample. In addition, both the granular simulations and laboratory experiments undergo roughly log-time compaction at comparable rates, when those rates are normalized by the appropriate value of D_c. For slide-hold-slide protocols, the granular model mimics laboratory experiments in that the rate of healing at sufficiently long hold times is roughly linear with log time, with a slope that is independent of the system stiffness and close to the RSF parameter b. Thus, despite several attributes that could be considered to be shortcomings, including the the use of spherical grains with a geologically narrow size distribution, the granular model still arguably does a better job of matching laboratory experiments than existing, and empirical, rate-state friction equations. The increase in apparent slip-weakening distance with hold duration is another feature the model shares with laboratory data but not the Slip law for state evolution, providing yet additional motivation for continuing to explore the granular model of fault friction.

Researchers in the fields of granular physics and granular rheology have previously found that the fluctuating kinetic energy, δE_k, sometimes referred to as the "granular temperature", in part controls the rheology of these materials in steady-state and some transient regimes (Kim & Kamrin, 2020; Gaume et al., 2020; Campbell, 1990). In our previous study, we found that although δE_k varied with confining pressure, the ratio of δE_k to elastic strain energy within the gouge varied only slightly with pressure and steady-state sliding speed, and was close to the (also nearly constant) value of the the direct velocity effect parameter a of the granular layer (Ferdowsi & Rubin, 2020). In that paper we evaluated the variation in fluctuating kinetic energy at steady-state shear velocities as low as 10^{-4} m/s. In the slide-hold simulations reported here, we find that δE_k becomes even more nearly constant down to transient sliding velocities below 10^{-7} m/s. We also find here that changing the damping (energy loss) for grain-grain interactions does not substantially alter the variation of δE_k, or the stress decay during holds, for the range of parameters explored. Further understanding what controls the changes in fluctuating kinetic energy, its near-constant value in the quasi-static limit, and its relation to the direct effect parameter a, may guide future studies of the proper formulations of rate-and-state friction laws for describing the transient frictional response of granular layers, and for connecting the RSF framework to more physics-based models.

Additional future research may explore recent definitions of state variable for amorphous materials (e.g., D. Richard et al. (2021)) in the context of elastoviscoplastic rheology for soft glassy materials (e.g., Fielding (2020)). These works may also address the applications of some of the latest developments in constitutive modeling of complex fluids with potentially similar (but as-yet unexplored in the context of rock and sediment friction) rate-dependent rheological response and hysteresis to rate- and state-dependent behavior of Earth materials.

of Vision Raytracer" POV-Ray (http://www.povray.org). Most of the data analysis were carried out using the open-source Python library, NumPy (https://numpy.org). The 2-D plots were made with the Python library Matplotlib (www.matplotlib.org). The computer codes for LAMMPS simulations of this paper with the information about the version of LAMMPS used for the simulations, are available on the Dryad digital repository at *https://doi.org/10.5061/dryad.2z34tmphk*. The views and conclusions contained in this document are those of the authors and should not be interpreted as necessarily representing the official policies, either expressed or implied, of the U.S. Government.

References

Abe, S., Dieterich, J. H., Mora, P., & Place, D. (2002). Simulation of the influence of rate-and state-dependent friction on the macroscopic behavior of complex fault zones with the lattice solid model. *pure and applied geophysics*, *159*(9), 1967–1983.

Ampuero, J.-P., & Rubin, A. M. (2008). Earthquake nucleation on rate and state faults–aging and slip laws. *Journal of Geophysical Research: Solid Earth*, *113*(B1).

Baumberger, T., Berthoud, P., & Caroli, C. (1999). Physical analysis of the state-and rate-dependent friction law. ii. dynamic friction. *Physical Review B*, *60*(6), 3928.

Baumberger, T., & Caroli, C. (2006). Solid friction from stick–slip down to pinning and aging. *Advances in Physics*, *55*(3-4), 279–348.

Beeler, N., Tullis, T., & Weeks, J. (1994). The roles of time and displacement in the evolution effect in rock friction. *Geophysical Research Letters*, *21*(18), 1987–1990.

Berthoud, P., Baumberger, T., G'sell, C., & Hiver, J.-M. (1999). Physical analysis of the state-and rate-dependent friction law: Static friction. *Physical review B*, *59*(22), 14313.

Bhattacharya, P., Rubin, A. M., Bayart, E., Savage, H. M., & Marone, C. (2015). Critical evaluation of state evolution laws in rate and state friction: Fitting large velocity steps in simulated fault gouge with time-, slip-, and stress-dependent constitutive laws. *Journal of Geophysical Research: Solid Earth*, *120*(9), 6365–6385.

Bhattacharya, P., Rubin, A. M., & Beeler, N. M. (2017). Does fault strengthening in laboratory rock friction experiments really depend primarily upon time and not slip? *Journal of Geophysical Research: Solid Earth*.

Bi, D., Henkes, S., Daniels, K. E., & Chakraborty, B. (2015). The statistical physics of athermal materials. *Annu. Rev. Condens. Matter Phys.*, *6*(1), 63–83.

Blanpied, M., Marone, C., Lockner, D., Byerlee, J., & King, D. (1998). Quantitative measure of the variation in fault rheology due to fluid-rock interactions. *Journal of Geophysical Research: Solid Earth*, *103*(B5), 9691–9712.

Blumenfeld, R., & Edwards, S. F. (2009). On granular stress statistics: Compactivity, angoricity, and some open issues. *The Journal of Physical Chemistry B*, *113*(12), 3981–3987.

Brilliantov, N. V., Spahn, F., Hertzsch, J.-M., & Pöschel, T. (1996). Model for collisions in granular gases. *Physical review E*, *53*(5), 5382.

Campbell, C. S. (1990). Rapid granular flows. *Annual Review of Fluid Mechanics*, *22*(1), 57–90.

Chen, J., & Spiers, C. J. (2016). Rate and state frictional and healing behavior of carbonate fault gouge explained using microphysical model. *Journal of Geophysical Research: Solid Earth*, *121*(12), 8642–8665.

Corwin, E. I., Jaeger, H. M., & Nagel, S. R. (2005). Structural signature of jamming in granular media. *Nature*, *435*(7045), 1075.

Dieterich, J. (1994). A constitutive law for rate of earthquake production and its application to earthquake clustering. *Journal of Geophysical Research: Solid Earth*, *99*(B2), 2601–2618.

Dieterich, J. H. (1972). Time-dependent friction in rocks. *Journal of Geophysical Research*, *77*(20), 3690–3697.

Dieterich, J. H. (1978). Time-dependent friction and the mechanics of stick-slip. In *Rock friction and earthquake prediction* (pp. 790–806). Springer.

Dieterich, J. H. (1979). Modeling of rock friction: 1. experimental results and constitutive equations. *Journal of Geophysical Research: Solid Earth*, *84*(B5), 2161–2168.

Dieterich, J. H. (1992). Earthquake nucleation on faults with rate-and state-dependent strength. *Tectonophysics*, *211*(1-4), 115–134.

Dieterich, J. H., & Kilgore, B. (1996). Implications of fault constitutive properties for earthquake prediction. *Proceedings of the National Academy of Sciences*, *93*(9), 3787–3794.

Dieterich, J. H., & Kilgore, B. D. (1994). Direct observation of frictional contacts: New insights for state-dependent properties. *Pure and Applied Geophysics*, *143*(1), 283–302.

Dieterich, J. H., et al. (1981). Constitutive properties of faults with simulated gouge. *Mechanical Behavior of*.

Ferdowsi, B., & Rubin, A. M. (2020). A granular-physics-based view of fault friction experiments. *Journal of Geophysical Research: Solid Earth*, e2019JB019016.

Fielding, S. M. (2020). Elastoviscoplastic rheology and aging in a simplified soft glassy constitutive model. *Journal of Rheology*, *64*(3), 723–738.

Gaume, J., Chambon, G., & Naaim, M. (2020). Microscopic origin of nonlocal rheology in dense granular materials. *Physical Review Letters*, *125*(18), 188001.

Handwerger, A. L., Rempel, A. W., Skarbek, R. M., Roering, J. J., & Hilley, G. E. (2016). Rate-weakening friction characterizes both slow sliding and catastrophic failure of landslides. *Proceedings of the National Academy of Sciences*, *113*(37), 10281–10286.

Hatano, T. (2009). Scaling of the critical slip distance in granular layers. *Geophysical Research Letters*, *36*(18).

Johnson, K. L. (1987). *Contact mechanics*. Cambridge University Press.

Kato, N., & Tullis, T. E. (2001). A composite rate-and state-dependent law for rock friction. *Geophysical research letters*, *28*(6), 1103–1106.

Kilgore, B. D., Blanpied, M. L., & Dieterich, J. H. (1993). Velocity dependent friction of granite over a wide range of conditions. *Geophysical Research Letters*, *20*(10), 903–906.

Kim, S., & Kamrin, K. (2020, Aug). Power-law scaling in granular rheology across flow geometries. *Phys. Rev. Lett.*, *125*, 088002. Retrieved from `https://link.aps.org/doi/10.1103/PhysRevLett.125.088002` doi: 10.1103/PhysRevLett.125.088002

Landau, L. D., & Lifshitz, E. M. (1959). Theory of elasticity.

Li, Q., Tullis, T. E., Goldsby, D., & Carpick, R. W. (2011). Frictional ageing from interfacial bonding and the origins of rate and state friction. *Nature*, *480*(7376), 233.

Liu, Y., & Szlufarska, I. (2012). Chemical origins of frictional aging. *Physical review letters*, *109*(18), 186102.

Losert, W., Bocquet, L., Lubensky, T., & Gollub, J. P. (2000). Particle dynamics in sheared granular matter. *Physical review letters*, *85*(7), 1428.

Marone, C. (1998). Laboratory-derived friction laws and their application to seismic faulting. *Annual Review of Earth and Planetary Sciences*, *26*(1), 643–696.

Marone, C., Raleigh, C. B., & Scholz, C. (1990). Frictional behavior and constitutive modeling of simulated fault gouge. *Journal of Geophysical Research: Solid Earth*, *95*(B5), 7007–7025.

Marone, C., & Saffer, D. (2015). The mechanics of frictional healing and slip instability during the seismic cycle. In G. Schubert (Ed.), *Treatise on geophysics (second edition)* (Second Edition ed., p. 111 - 138). Oxford: Elsevier. Retrieved from `http://www.sciencedirect.com/science/article/pii/B9780444538024000920` doi: https://doi.org/10.1016/B978-0-444-53802-4.00092-0

McCarthy, C., Savage, H., & Nettles, M. (2017). Temperature dependence of ice-on-rock friction at realistic glacier conditions. *Philosophical Transactions of the Royal Society A: Mathematical, Physical and Engineering Sciences*, *375*(2086), 20150348.

MiDi, G. (2004). On dense granular flows. *European Physical Journal E–Soft Matter*, *14*(4).

Mindlin, R. D. (1949). Compliance of elastic bodies in contact. *J. Appl. Mech., ASME*, *16*, 259–268.

Morgan, J. K. (2004). Particle dynamics simulations of rate-and state-dependent frictional sliding of granular fault gouge. In *Computational earthquake science part i* (pp. 1877–1891). Springer.

Nagata, K., Nakatani, M., & Yoshida, S. (2012). A revised rate-and state-dependent friction law obtained by constraining constitutive and evolution laws separately with laboratory data. *Journal of Geophysical Research: Solid Earth*, *117*(B2).

Nakatani, M. (2001). Conceptual and physical clarification of rate and state friction: Frictional sliding as a thermally activated rheology. *Journal of Geophysical Research: Solid Earth*, *106*(B7), 13347–13380.

Ono, I. K., O'Hern, C. S., Durian, D. J., Langer, S. A., Liu, A. J., & Nagel, S. R. (2002). Effective temperatures of a driven system near jamming. *Physical review letters*, *89*(9), 095703.

Plimpton, S. (1995). Fast parallel algorithms for short-range molecular dynamics. *Journal of computational physics*, *117*(1), 1–19.

Puckett, J. G., & Daniels, K. E. (2013). Equilibrating temperaturelike variables in jammed granular subsystems. *Physical Review Letters*, *110*(5), 058001.

Richard, D., Kapteijns, G., Giannini, J. A., Manning, M. L., & Lerner, E. (2021, Jan). Simple and broadly applicable definition of shear transformation zones. *Phys. Rev. Lett.*, *126*, 015501. Retrieved from `https://link.aps.org/doi/10.1103/PhysRevLett.126.015501` doi: 10.1103/PhysRevLett.126.015501

Richard, P., Artoni, R., Valance, A., & Delannay, R. (2020). Influence of lateral confinement on granular flows: comparison between shear-driven and gravity-driven flows. *Granular Matter*, *22*(4), 1–13.

Ruina, A. (1983). Slip instability and state variable friction laws. *Journal of Geophysical Research: Solid Earth (1978–2012)*, *88*(B12), 10359–10370.

Silbert, L. E., Ertaş, D., Grest, G. S., Halsey, T. C., Levine, D., & Plimpton, S. J. (2001). Granular flow down an inclined plane: Bagnold scaling and rheology. *Physical Review E*, *64*(5), 051302.

Sleep, N. H. (2006). Real contacts and evolution laws for rate and state friction. *Geochemistry, Geophysics, Geosystems*, *7*(8).

Song, C., Wang, P., & Makse, H. A. (2005). Experimental measurement of an effective temperature for jammed granular materials. *Proceedings of the National Academy of Sciences*, *102*(7), 2299–2304.

Thom, C., Carpick, R., & Goldsby, D. (2018). Constraints on the physical mechanism of frictional aging from nanoindentation. *Geophysical Research Letters*, *45*(24), 13–306.

Tian, K., Goldsby, D. L., & Carpick, R. W. (2018). Rate and state friction relation for nanoscale contacts: Thermally activated prandtl-tomlinson model with chemical aging. *Physical Review Letters*, *120*(18), 186101.

Tian, K., Gosvami, N. N., Goldsby, D. L., Liu, Y., Szlufarska, I., & Carpick, R. W. (2017). Load and time dependence of interfacial chemical bond-induced friction at the nanoscale. *Physical review letters*, *118*(7), 076103.

Viesca, R. C. (2016). Self-similar slip instability on interfaces with rate-and state-dependent friction. *Proceedings of the Royal Society A: Mathematical, Physical and Engineering Sciences*, *472*(2192), 20160254.

Zhang, H., & Makse, H. (2005). Jamming transition in emulsions and granular materials. *Physical Review E*, *72*(1), 011301.